Characterization of Titanium Dioxide Blocking Layers in Dye-Sensitized Nanocrystalline Solar Cells

Petra J. Cameron and Laurence M. Peter*

Department of Chemistry, University of Bath, Bath BA2 7AY, United Kingdom

Received: June 25, 2003; In Final Form: October 2, 2003

The properties of thin blocking layers of titanium dioxide used to improve the performance of dye-sensitized nanocrystalline solar cells have been studied. TiO_2 blocking layers prepared on fluorine-doped tin oxide-coated glass by spray pyrolysis have been characterized by electrochemical impedance spectroscopy, spectroscopic ellipsometry, and voltammetry. The impedance data reveal the presence of a distribution of surface states at the titanium dioxide−electrolyte interface that is similar to the one seen in the case of nanocrystalline TiO_2 films. The influence of the blocking layers on the back transfer of electrons to tri-iodide ions in electrolyte-based dye-sensitized nanocrystalline cells has been studied by open circuit photovoltage decay. The results show that the ability of the blocking layer to prevent the back reaction of electrons with tri-iodide ions in the electrolyte is excellent under short circuit conditions, but is limited under open circuit conditions by electron accumulation at the surface of the titanium dioxide blocking layer.

Introduction

Identification of the factors limiting the performance of dye-sensitized nanocrystalline solar cells (DSSC)[1] is a key objective of current research, as attempts are made to increase the AM 1.5 solar power efficiency of these cells beyond 10%.[2,3] At the same time, solid-state analogues of liquid-electrolyte DSSCs are beginning to achieve respectable efficiencies. In these cells, the iodide−tri-iodide electrolyte is replaced by a hole-conducting phase such as spiro-MeOTAD (2,2′,7,7′-tetrakis(*N*,*N*-di-*p*-methoxyphenylamine)-9,9′-spirobifluorene).[4] In the case of these solid-state cells, it has been demonstrated that the fluorine-doped tin oxide (FTO) substrates must be covered by a thin blocking layer of titanium dioxide[5] in order to prevent efficiency loss due to electron transfer to the hole-conducting medium from the FTO, which typically has a doping density in excess of 10^{20} cm^{-3}. Spray-pyrolysis[6] has been used to coat the FTO−glass substrates with thin films of titanium dioxide that allow photoinjected electrons to be collected from the light-harvesting film of sensitized nanocrystalline TiO_2 but prevent escape of electrons from the FTO substrate to the hole-conducting polymer (interfacial electron−hole recombination).[5] Here we focus on the influence of blocking layers on back transfer of electrons in electrolyte-based DSSCs.

The nature of the three-phase contact, FTO, TiO_2, electrolyte in DSSCs is still not well understood. It is clear that it must allow electrons to be extracted efficiently from the nanocrystalline TiO_2 layer, but transfer of electrons to the electrolyte phase should be inhibited.[7] This becomes particularly important if the iodide−tri-iodide redox mediator is replaced by a one-electron redox couple.[8] Figure 1 illustrates schematically the two routes for electron transfer to redox ions in the electrolyte—via the nanocrystalline TiO_2 and via the conducting FTO substrate. Electron transfer via both routes needs to be minimized in order to prevent the loss of photoinjected electrons by back reaction. In the case of cells based on the iodide-tri-iodide couple, it is commonly assumed that transfer of electrons via the FTO substrate is negligible since the I_3^-−I^- exchange current density is very small. It is certainly reasonable to neglect losses via the FTO under short circuit conditions, because the Fermi level in the FTO is close to the redox Fermi level. However, in the nanocrystalline TiO_2 layer, the quasi-Fermi level under illumination rises rapidly with distance from the substrate as illustrated in Figure 2a, so that the driving force for electron transfer of electrons from the TiO_2 nanoparticles to I_3^- in the electrolyte is much greater in the bulk of the sensitized layer than close to the FTO substrate. As a consequence, the back reaction of electrons with I_3^- *at short circuit* is expected to occur predominantly in the bulk of the nanocrystalline TiO_2.

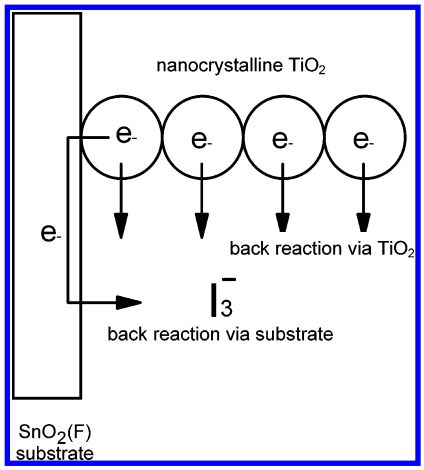

Figure 1. Schematic illustration of the direct route for electron transfer to I_3^- via the nanocrystalline TiO_2 with the indirect route via the conducting glass substrate. The second route is expected to become important under open circuit conditions (see Figure 2).

The situation is different under open circuit illumination conditions. The Fermi level of the FTO substrate typically rises by up to 0.7 eV as illustrated in Figure 2b, so that there is now a much larger driving force for electron transfer from the FTO

* Corresponding author. Tel: +44 1225 386815. Fax: +44 1225 385802. E-mail: l.m.peter@bath.ac.uk.

10.1021/jp030790+ CCC: $25.00
Published on Web 12/02/2003

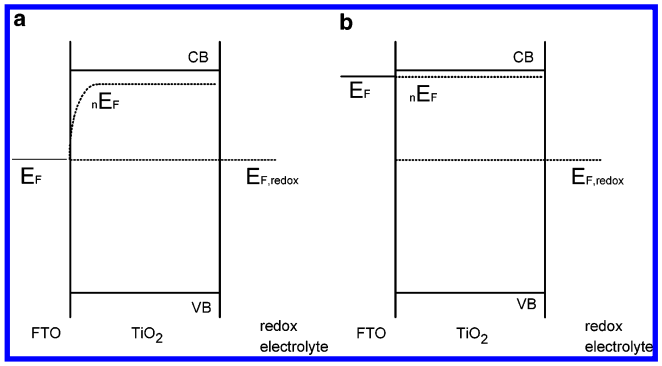

Figure 2. Schematic description of the illuminated DSSC in the absence of a blocking layer. The TiO_2 label refers to the layer of dye-sensitized nanocrystalline TiO_2. (a) Under short circuit conditions the Fermi level in the FTO is pinned close to the redox Fermi level as a consequence of the rapid electron-transfer kinetics at the platinum counter electrode. The electron quasi Fermi level ($_nE_F$) in most of the nanocrystalline film is much higher than at the FTO contact, so that electron transfer to I_3^- takes place predominantly in the bulk of the porous film. (b) Under open circuit conditions, the Fermi level in the FTO moves up as the electron quasi Fermi level in the nanocrystalline film rises due to the establishment of a photostationary state in which the rate of electron injection by the sensitizer dye is balance by the back transfer of electrons to I_3^- by the two routes identified in Figure 1.

to I_3^-. Under these conditions, the back reaction of electrons with I_3^- via the FTO will no longer be negligible, so that both routes will contribute to the establishment of the photostationary state. It is worth noting that the boundary condition commonly used for open circuit conditions is the net electron flux across the TiO_2-SnO_2 interface is zero. In fact, this is incorrect, and it should be replaced by the boundary condition that the flux of electrons across the TiO_2-SnO_2 interface is balanced by the flux of electrons across the exposed SnO_2-electrolyte interface between the particles.

Clearly, the thickness, doping density, and band alignment of titanium dioxide blocking layers on FTO are likely to be factors that play a critical role in their performance. The aim of the present study was to evaluate the relative importance of the two back-reaction routes identified in Figure 1 and to examine the ability of blocking layers to prevent or reduce losses arising from electron transfer via the substrate. The results show that titanium dioxide blocking layers prepared by spray pyrolysis are n-doped but are not degenerately doped (n^+) like the FTO substrate. The electron density at the TiO_2-electrolyte interface will depend on doping density and on the band bending in the TiO_2 film, which is controlled by the photovoltage in the DSSC. The results presented here show that under strong illumination at open circuit or on load, the TiO_2 blocking film is driven toward the flatband condition, so that electron transfer to I_3^- becomes possible and the films can no longer be described as "blocking".

Experimental Section

Compact TiO_2 blocking layers were deposited by spray-pyrolysis using a hand-held atomizer, following the method developed by Kavan and Grätzel.[9] A solution of 0.2 M titanium di-isopropoxide bis(acetylacetonate) (Aldrich) in 2-propanol was sprayed in very short pulses of 1 s duration onto a clean conducting glass substrate (FTO: fluorine-doped tin oxide-coated glass, Hartford Glass, USA, sheet resistance 15 Ω □) placed on a hotplate at 450 °C. The overall thickness of the films deposited under identical conditions on 1 mm thick glass microscope slides was determined by spectroscopic ellipsometry over the wavelength range 200 to 1000 nm using a spectroscopic ellipsometer (J. A. Woollam M2000U). The ellipsometric parameters Ψ and Δ were measured as a function of wavelength for both bare glass substrate and TiO_2-coated substrates at incident angles of 65°, 70°, and 75°. The ellipsometric results were fitted to a 2-layer model (glass-slide$-TiO_2$) using the V.A.S.E software package. The TiO_2 films were modeled with a Tauc-Lorentz oscillator model to obtain a best fit for fit thickness and optical constants. Values of the TiO_2 film thickness ranging between 56 and 118 nm were obtained, although it proved difficult to establish a reproducible correlation between the number of spray pulses and the film thickness.

The TiO_2-coated plates were divided into three groups. The first set of samples was used to make dye-sensitized nanocrystalline cells. Plates in the second set were fabricated into thin layer cells without any sensitized nanocrystalline TiO_2 overlayer. Plates in the third set were used without further modification for capacitance−voltage measurements. Dye-sensitized cells were fabricated by doctor-blading aqueous TiO_2 colloid made by the nitric acid hydrolysis route [10] onto cleaned FTO glass or FTO glass precoated with spray-pyrolyzed TiO_2. The coated plates were then fired in air at 450° C for 30 min. The thickness of the nanocrystalline TiO_2 layers was in the range 4−5 μm, and the active area of the cells was 1 cm^2. After the heat treatment of the nanocrystalline films, dye loading was performed by immersion in 0.3 mM *cis*-di(thiocyanato)-*N*,*N*-bis-(2,2′-bipyridyl dicarboxylate) ruthenium(II) (Solaronix) in anhydrous ethanol for 15 h. The film was then washed with anhydrous ethanol and dried under a stream of nitrogen. The second half of the sandwich cell, consisting of an FTO glass plate coated with a sputter-deposited layer of platinum, was heat-sealed on with 50 μm Surlyn gasket. The electrolyte, which was composed of 0.85 M methylhexylimidazolium iodide, 0.05 M iodine (anhydrous 99.999%, Aldrich), 0.1 M LiI (anhydrous 99.999%, Aldrich), and 0.2 M *tert*-butylpyridine (Aldrich, 99%) in acetonitrile, was introduced into the cell through holes drilled in the counter electrode, which were subsequently heat-sealed with glass cover slips using Surlyn.

Thin layer electrochemical cells were made in the same way as the DSSC, except that the sensitized nanocrystalline TiO_2 layer was omitted. The first cell contained an uncoated FTO working electrode and a Pt-coated counter electrode. The working electrodes of the remaining three cells consisted of FTO glass covered with TiO_2 blocking layers produced by 36, 60, and 84 spray pulses, respectively.

Flatband potentials and doping densities of the compact underlayers of TiO_2 were determined using capacitance−voltage data derived from the EIS response measurements using the DSSC electrolyte as well as aqueous 0.1 M Na_2SO_4 (pH 3). For the three-electrode measurements in Na_2SO_4, a 1 cm^2 area of the TiO_2-coated FTO glass served as the working electrode and a platinum foil counter electrode and Ag/AgCl reference electrode (CH instruments) completed the cell. Linear sweep voltammetry and EIS measurements were carried out using an Autolab PGSTAT12 with an internal frequency response analyzer (Eco Chemie BV). The frequency-dependent impedance was fitted using NLS software (Solartron Z-view) to obtain the space charge capacitance of the uncoated and TiO_2-coated FTO electrodes. Open circuit photovoltage decay measurements were carried out using an apparatus that has been described elsewhere.[11,12]

Results and Discussion

Voltammetry. The thin layer cells with Pt counter electrodes were used to study the electrochemical behavior of the $I_3^-I^-$

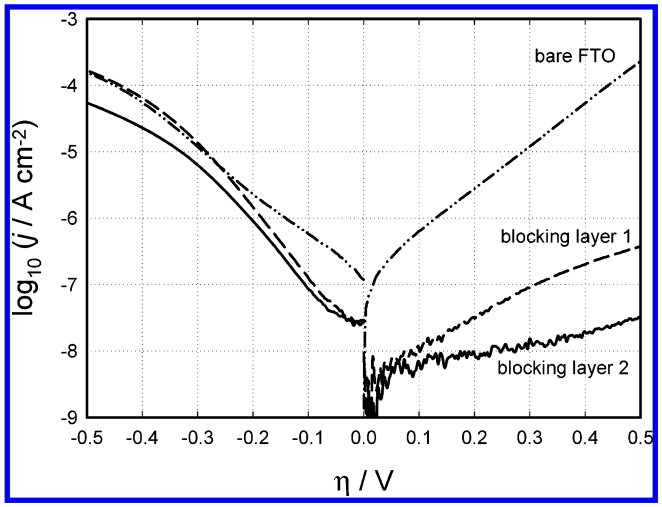

Figure 3. Current voltage characteristics of thin layer cells containing the DSSC electrolyte. The counter electrode is platinum in each case. In the case where the working electrode is uncoated FTO, the symmetrical $j-V$ curves indicate facile electron transfer in both the anodic and cathodic regimes, showing that electron tunneling through the thin space charge region occurs. The anodic branch of the $j-V$ plots is strongly suppressed when a blocking layer of TiO_2 is used. By contrast, the effect on the cathodic branch is less marked, particularly in the case of the thinner of the two blocking layers (1).

redox couple at coated and uncoated FTO. Four cells were used, one with a bare FTO working electrode and three with spray-pyrolyzed TiO_2 coatings on the FTO (prepared by 36, 60, and 84 pulses, respectively). The uppermost I−V plot in Figure 3 illustrates the current voltage behavior of the uncoated FTO electrode. Since the exchange current density of the I^-/I_3^- couple is known to be high at the platinum and the regenerative thin layer cell configuration minimizes the effects of diffusive transport, the response of the two electrode thin layer cell is dominated by the much slower kinetics of electron transfer at the FTO electrode (we assume that the Pt electrode remains close to the equilibrium potential, provided that the cell current does not approach the diffusion controlled limit). It can be seen from the plot for FTO in Figure 3 that oxidation of I^- occurs at potentials more positive than the equilibrium potential. There is no evidence that the formation of a depletion layer in the FTO film significantly inhibits electron transfer, indicating that facile electron tunneling occurs through the very thin depletion layer of the n^+-doped SnO_2. As expected, reduction of I_3^- to I^- occurs at negative potentials. Figure 3 shows that the exchange current density, j_0, for the I^-/I_3^- couple at the FTO electrode is only 10^{-7} A cm^{-2}. This is much lower than j_0 for the same redox electrolyte at platinum, which we estimate from impedance measurements to be 4 to 5 orders of magnitude larger.

Figure 3 also illustrates the current−voltage characteristics of two of the TiO_2 blocking layers. The most striking effect is the almost total suppression of I^- oxidation. By contrast, the effect on the reduction of I_3^- is much less marked, particularly in the case of the thinner blocking film. This "diode" behavior suggests that the TiO_2 film is in depletion in the potential region where I^- could be oxidized, so that electron transfer to the underlying FTO is inhibited by the presence of a space charge layer in the TiO_2 that is sufficiently wide to hinder electron tunneling from I^- to the conduction band. The very low values of current in this potential region also show that the TiO_2 film is virtually free of cracks or pores that penetrate to the underlying highly doped FTO substrate.

Figure 3 shows that the blocking layer is much less efficient at potentials negative of the equilibrium I_3^-/I^- potential. When the potential becomes more negative than −0.2 V, the current for both coated electrodes rises in a way that suggests that the electron density in the interface between the TiO_2 blocking layer and the redox electrolyte increases as the band bending in the TiO_2 decreases.

Electrochemical Impedance Spectroscopy (EIS). To determine the flatband potential and doping density of the TiO_2 blocking layers, electrochemical impedance spectroscopy (EIS) was used to derive values of the space charge capacitance as a function of potential for the construction of Mott Schottky plots. Capacitance data derived by fitting the EIS data are more reliable than those obtained from single frequency measurements since, as is evident from the Tafel plots, the Faradaic contribution to the interfacial impedance in the DSSC electrolyte cannot be neglected, particularly at negative applied potentials. The impedance results also indicated a high density of surface states at the TiO_2−organic electrolyte interface. Impedance measurements were also carried out using aqueous Na_2SO_4 electrolyte, and in this case complications due to Faradaic processes and interference from surface states were both found to be negligible. Although the Mott Schottky plots for the data obtained using aqueous solutions are not shown here, they gave doping density values that agreed very well with those derived from the EIS analysis of the thin film cells containing the organic electrolyte. This gives us confidence that the deconvolution of the EIS data has been performed satisfactorily.

Figure 4a shows the impedance response of an FTO electrode coated with a blocking layer measured at zero applied voltage, i.e., at the electrode poised at the reversible I_3^-/I^- potential. As indicated by the phase angle in the Bode plot, the coated electrode exhibits essentially capacitive behavior at low frequencies. This is confirmed by the complex plane plot shown in the inset. The capacitive behavior at 0 V is consistent with the low exchange current density seen in the Tafel plots: the Faradaic impedance is greater than 10^6 Ω cm^2. However, the additional maximum seen in the phase angle at higher frequencies indicates the presence of additional impedance components.

The impedance of the same TiO_2-coated electrode at −0.5 V is illustrated by the Bode plot in Figure 4b, and the corresponding complex plane plot is shown in the inset. The low-frequency behavior is now different. The phase angle tends to zero, since electron transfer to I_3^- gives rise to a Faradaic resistance in parallel with the capacitance of the electrode. This corresponds to the semicircular response in the complex plane. Figures 4b and 4c both reveal the presence of a second time constant in the impedance response at high frequencies. This gives rise to the second maximum in the phase angle (at around 2 kHz) and to the additional small semicircle at high frequencies in the complex plane plot shown in the inset to Figure 4b. An ideal semiconductor−electrolyte interface is expected to give rise to a single semicircle in the complex plane impedance plot. The experimental impedance responses described here are characteristic of a nonideal semiconductor−electrolyte interface with surface states. The impedance data were therefore fitted to the equivalent circuit shown in Figure 5.

Here, R_0 is the ohmic resistance of the FTO substrate electrode, C_{SC} and R_{SC} are the space charge capacitance and resistance, respectively, and C_{SS} and $R_{SS,}$ are the surface state capacitance and resistance, respectively. R_{SC} is related to the transfer of electrons across the film−solution interface, and it is related to the exchange current density and Tafel slopes by

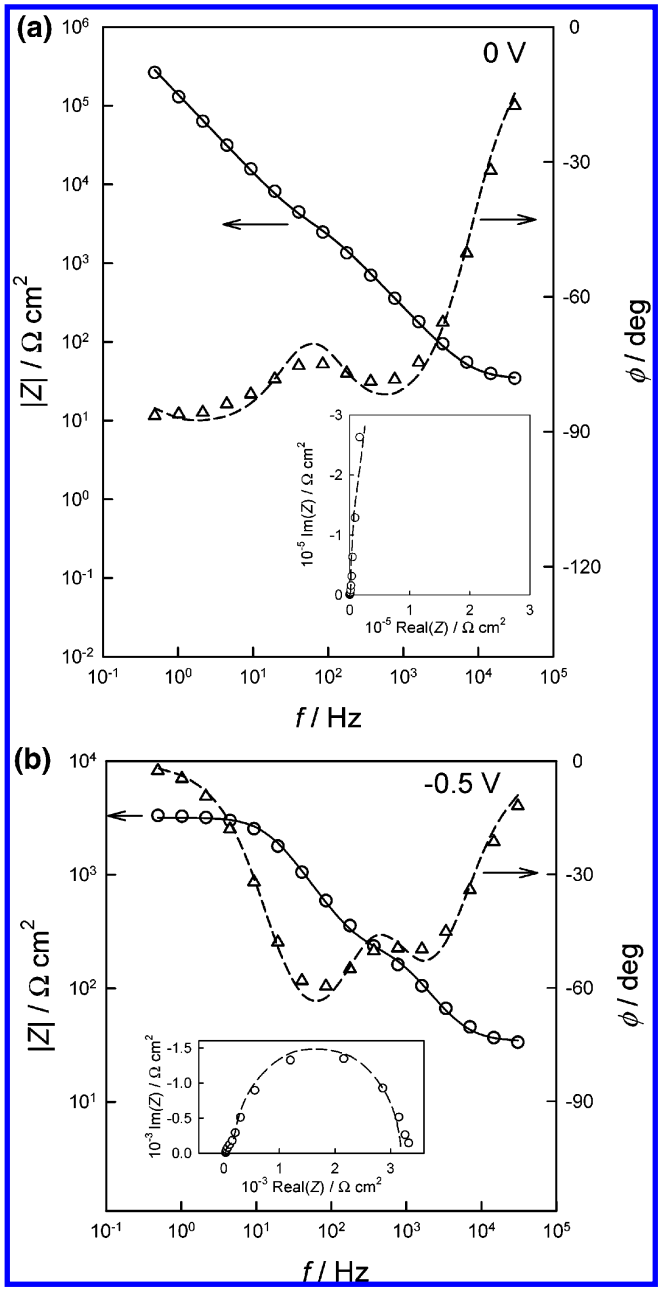

Figure 4. Impedance behavior of a thin layer cell with a blocking layer of TiO_2. (a) Response at 0 V, i.e., the working electrode is at the equilibrium I_3^-−I^- potential. The Bode plots indicate that the impedance is capacitive at low frequencies. This is confirmed by the complex plane plot shown in the insert. The maximum in the phase angle seen at higher frequencies indicates nonideal behavior arising from surface states. The lines are the fits obtained using the equivalent circuit shown in Figure 5. (b) Response at −0.5 V. The low-frequency impedance is now resistive due to electron transfer to I_3^-. The complex plane plot shows a small semicircle at high frequencies in addition to the simple semicircle expected for an ideal interface free of surface states. This nonideality is also evident in the Bode plot, which shows a second maximum in the phase angle. The lines are the fits to the equivalent circuit shown in Figure 5.

the expression

$$R_{SC} = \frac{|j|\alpha q}{k_B T} \tag{1}$$

Here, α is transfer coefficients for the anodic or cathodic process, and j is the current density at a particular potential. C_{SS} is related to the density of states function for surface states,

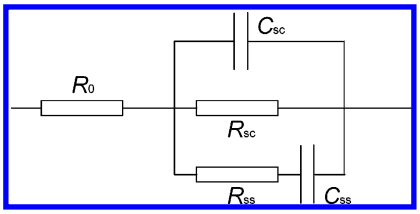

Figure 5. Equivalent circuit used to fit the EIS data. R_0 is the resistance of the FTO-coated glass electrode, C_{SC} is the space charge capacitance, R_{SC} is the resistance associated with electron exchange with redox species, C_{SS} is the surface state capacitance, and R_{SS} determines the time constant for electron exchange with the surface states via the time constant $\tau_{SS} = R_{SS}C_{SS}$.

$N_{SS}(E)$ by

$$C_{SS}(\eta) = qN_{SS}(E_F - E_{F,redox}) \tag{2}$$

Here, η is the overvoltage with respect to the equilibrium potential of the redox couple, and $E_F - E_{F,redox}$ is the corresponding energy difference. Note that $N_{ss}(E)$ has dimensions cm^{-2} eV^{-1}.

The product $R_{SS}C_{SS} = \tau_{SS}$ is the time constant associated with electron exchange between the surface states and the conduction band. In simple models, τ_{SS} is considered to be determined by the energy depth of the surface state relative to the conduction band edge, but it is probably more realistic to consider that it will depend in a complex way on the interaction of trapped charges with ions and dipoles in the adjacent electrolyte phase.

The fitting of the impedance data is illustrated in Figures 4a and 4b. In the fits shown, no attempt has been made to account for the effects of surface inhomogeneity by introducing constant phase shift elements (CPEs) in place of C_{SC} and C_{SS}. Not surprisingly, improved fits are obtained using CPEs, but their inclusion provides no new physical insights. Values of all of the components of the equivalent circuit in Figure 5 were derived over the potential range from 0.5 V to −0.5 V vs I_3^-−I^-. Figures 6a and 6b show the potential dependence of the capacitance and resistance elements. The values of C_{SC} derived from the EIS analysis were also used to construct the Mott Schottky plot included in Figure 6a. The flatband potential of the TiO_2 blocking layer is seen to be −0.76 V. This value of E_{fb} is consistent with the photovoltages of the DSSCs based on this electrolyte, which are less than 0.7 V. The doping density of the film estimated from the slope of the plot (using a surface roughness factor of 1.5[13] and $\epsilon_{TiO_2} = 40$) is 1.7×10^{18} cm^{-3}.

It can be seen that the Mott Schottky plot in Figure 6a begins to saturate at high values of band bending. We have shown elsewhere that this is characteristic of thin films in which the space charge region extends to the back conatact.[13] A rough estimate based on the same values of surface roughness factor and relative permittivity gave a film thickness of 50 nm, which is in reasonable agreement with the thickness derived by ellipsometry.

The potential dependence of C_{SS} and τ_{SS} are shown in the semilogarithmic plots in Figure 7. The right-hand axis shows the corresponding state density of surface states. The density of states distribution can be approximated by an expression of the form

$$N_{SS}(E_F - E_{F,redox}) = N_{SS}(0)\exp\left[\frac{\beta(E_F - E_{F,redox})}{k_B T}\right] \tag{3}$$

with $\beta = 0.16$. This distribution of surface is remarkably similar to the one derived for nanocrystalline TiO_2 in the same electrolyte from photopotential decay and charge extraction

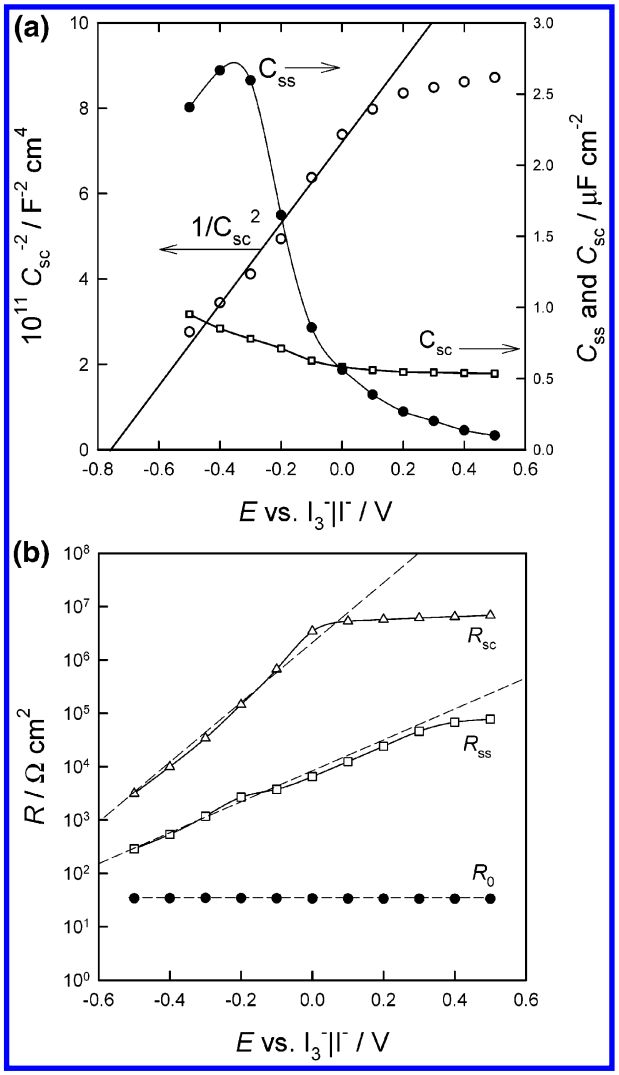

Figure 6. (a) Potential dependence of C_{SC} and C_{SS} derived from the EIS analysis. The figure also shows the Mott Schottky plot constructed using the C_{SC} values. Values of the doping density and flatband potential are given in the text. Note the steep rise in C_{SS} as the potential becomes more negative. This corresponds to an increase in surface state density as the Fermi level approaches the conduction band of TiO_2 (see also Figure 7). Note also the saturation of the Mott Schottky plot, which is attributed to the extension of the space charge region throughout the whole of the TiO_2 film. (b) Potential dependence of R_0, R_{SC}, and R_{SS}.

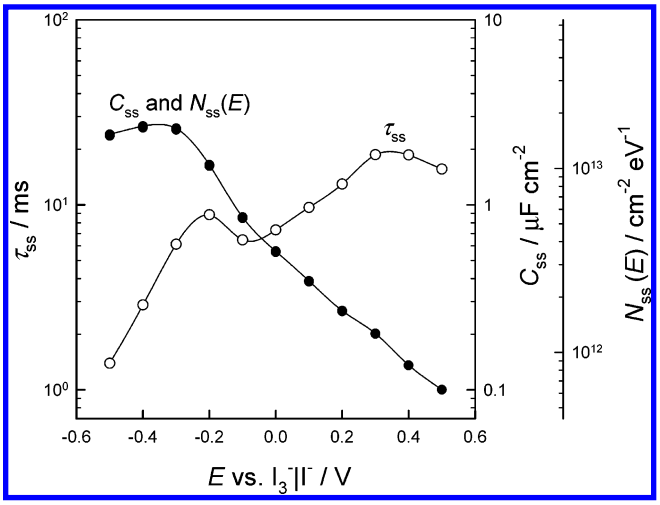

Figure 7. Semilogarithmic plots showing the potential dependences of C_{SS} and τ_{SS}. The variation of C_{SS} is consistent with an exponential energy distribution of surface states (see text for details). The variation of τ_{SS} indicates that electron exchange between the surface states and the conduction band does not follow simple Boltzmann behavior.

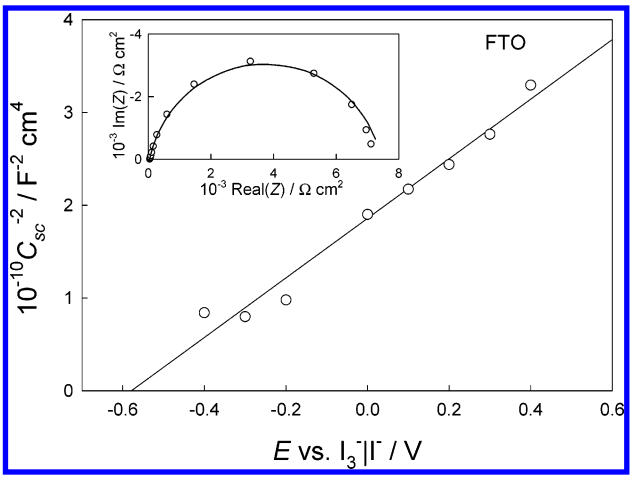

Figure 8. Mott Schottky plot for uncoated FTO in DSSC electrolyte derived from the EIS analysis. Values of the doping density and flatband potential are given in the text. The inset shows a complex plane impedance plot for the FTO electrode at −0. 5 V. Note the simple *RC* behavior (compare Figure 4b).

measurements that have been reported elsewhere.[11,14] It is interesting to note that the surface state density in aqueous Na_2SO_4 is so low that no surface state capacitance can be detected. This suggests that the surface states are extrinsic, i.e., that they arise from interactions between the TiO_2 surface and components of the electrolyte. The integrated capacitance gives the total number of surface states between +0.5 V and −0.5 V and also gives the surface charge, Q_{surf}, from which the corresponding change in potential drop across the Helmholtz layer can be calculated: $\Delta V_H = Q_{surf}/C_H$. The band edge unpinning due to surface charging is estimated to be 0.15 meV at −0.5 V.

In the case of FTO electrodes, the high-frequency response did not reveal the presence of a second time constant, so that C_{SS} and R_{SS} were omitted from the equivalent circuit when modeling impedance data for uncoated electrodes. The complex plane impedance plot shown as an inset in Figure 8 illustrates the results of fitting the impedance response of the uncoated FTO electrode. The voltage dependence of the space charge capacitance of the FTO is displayed in the form of a Mott Schottky plot in Figure 8. A doping density of 10^{20} cm^{-3} was derived from this plot by assuming a surface roughness factor of 1.5[13] and $\epsilon_{SnO_2} = 10$. Exact determination of the flatband potential of the FTO is complicated by the fact that it is necessary to correct for the Helmholtz capacitance, C_H, in the case of highly doped semiconductors. If we assume $C_H = 10$ μF cm^{-2}, the flatband potential is estimated to be −0.5 V vs I_3^-−I^-.

The Faradaic admittance derived from the EIS analysis for electrodes with and without TiO_2 blocking layers are compared in Figure 9 as semilogarithmic plots that can be compared with the corresponding Tafel plots in Figure 3. The slopes of the semilogarithmic plots of R_f^{-1} vs potential are equivalent to the conventional Tafel slopes. In the present case, the cathodic and anodic slopes for uncoated FTO agree very well with the Tafel slopes measured for the FTO electrode (see Figure 3). The results confirm that the FTO electrode behaves essentially as a metal as far as electron transfer is concerned, although a well-behaved depletion region can be identified from the Mott Schottky plot in Figure 8. Clearly electron tunneling through the thin space charge region is sufficiently facile to give "metallic" electron-transfer behavior. By contrast, the TiO_2-coated electrode shows strong blocking behavior in the anodic

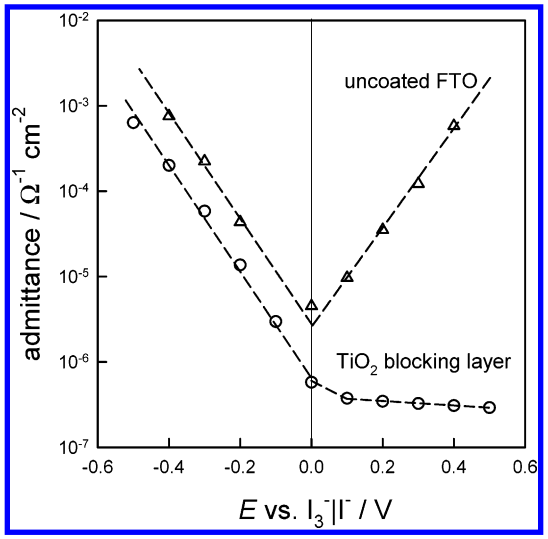

Figure 9. Potential dependence of the electrode admittance for uncoated and coated FTO electrodes in thin layers cells. The plots are consistent with the $j-V$ plots shown in Figure 3. Note in particular the decrease in admittance in the anodic region for the FTO electrode coated with a TiO_2 blocking layer.

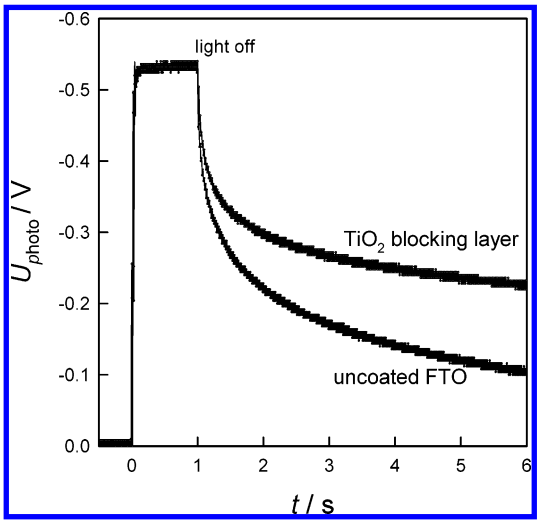

Figure 10. Plots contrasting the decay in photovoltage for DSSCs with and without blocking layers (LED illumination). Note the similarity in initial decay behavior and the large difference at longer times, showing that electron transfer occurs at the uncoated FTO electrodes.

region, but only relatively weak attenuation of the current in the cathodic region.

The properties of the blocking TiO_2 layers in dye-sensitized cells were examined by the comparing the open circuit photovoltage decay curves for cells with and without the layers under the nanocrystalline light-harvesting film. Figure 10 shows that the blocking layers strongly influence the slow decay component of the photovoltage decay. By contrast, the initial rapid decay of the photovoltage is much less sensitive to the presence of a blocking layer. The decay of the photovoltage reflects the decrease in the concentration of electrons in the conduction band of the nanocrystalline TiO_2 particles immediately adjacent to the substrate contact. This electron density, $n_{x=0}$ determines the local quasi-Fermi energy, ${}_nE_F$:

$$n_{x=0} = N_C \exp\left(-\frac{{}_nE_F - E_C}{k_B T}\right) \quad (4)$$

where N_C is the effective density of states in the conduction

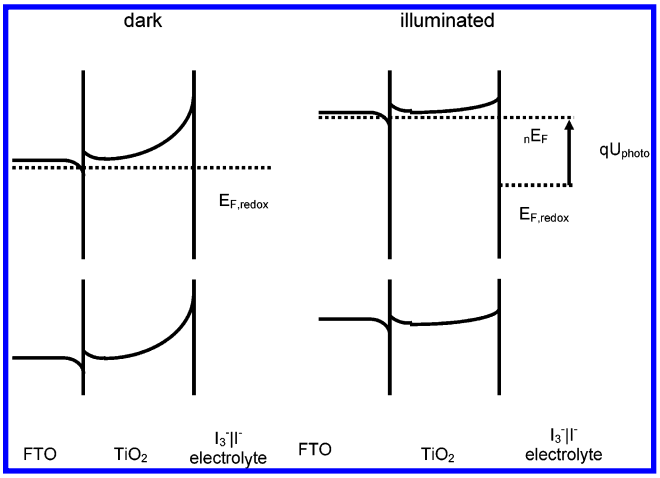

Figure 11. Schematic diagrams of the FTO−TiO_2 electrolyte junctions under open circuit conditions in the dark and under illumination. See text for details.

band. The electron density falls when the illumination is interrupted because electrons can be transferred to I_3^- ions (cf. Figure 1). The fact that the rapid initial photovoltage decay is very similar for cells with and without blocking films indicates that electron transfer in this region of the photovoltage decay curve is not affected by the TiO_2 blocking layer. By contrast, the photovoltage decay at longer times (i.e., lower photovoltages) is much slower for the cell with a blocking layer. This indicates that the transfer of electrons responsible for the lowering of ${}_nE_F$ in a cell without a blocking layer occurs at least partly via the exposed SnO_2(F) substrate. This is consistent with the current−voltage plots shown in Figure 2, which show that at less negative potentials (i.e., lower photovoltages in the present case), the TiO_2 layers begin to block electron transfer to I_3^-.

A number of open questions remain about the nature of the junctions between the FTO and the TiO_2 blocking layer and between the blocking layer and the nanocrystalline TiO_2 particles in the DSSC. The mismatch in electron affinity of TiO_2 and SnO_2 may lead to the formation of a conduction band spike at the interface between the FTO and the blocking layer. Figure 11 is a schematic representation of the band structure of the junction with a blocking layer under open circuit conditions (for simplicity, the nanocrystalline TiO_2 layer is now shown). It has been assumed that the electron affinity mismatch leads to a small conduction band spike (if such a spike is present, it does not significantly impede electron extraction from the DSSC). In the dark, the Fermi level is uniform throughout the system. Under illumination at open circuit, the electron quasi Fermi level in the nanocrystalline TiO_2 layer rises as shown, giving rise to a photovoltage. Since electrons in the solid phases can equilibrate, the Fermi level in the blocking layer rises as well, and the band bending is reduced correspondingly. It can be seen that when the cell is at open circuit (or on load), the surface electron density in the blocking films increases along with the driving force for electron transfer to I_3^-. Consequently the blocking behavior is no longer evident to the same extent. This conclusion is consistent with the photovoltage decay curves in Figure 10, which indicate that the TiO_2 films no longer block effectively when the photovoltage exceeds 400 mV.

The information about the potential-dependent current densities for FTO-coated glass with and without blocking layers obtained from the thin layer cell measurements has been used as input data for a model of the photovoltage decay that takes into account the two pathways for electron transfer shown in

Figure 1. Details of the model, which also considers discharge of the substrate capacitance as well as electron transfer via the substrate and the nanocrystalline TiO_2 layer, lie outside the scope of the present paper and will be given elsewhere.[15]

Conclusion

This study has shown that the blocking properties of thin titanium dioxide films are determined by the formation of a depletion region. Although the films exhibit diode behavior, the doping densities are too high to guarantee effective blocking of electron transfer to the redox system at cell voltages in the region of the maximum power point. The exchange current density of the I_3^-−I^- couple at the TiO_2 film is less than an order of magnitude lower than at n^+ FTO electrodes, and the difference in current density for tri-iodide reduction is even smaller at more negative potentials approaching the open circuit voltage. Films with lower doping densities would be preferable, particularly for one-electron-transfer systems or hole-conducting polymers that have higher exchange current densities than the I_3^-−I^- redox couple. Work is in progress to extend the characterization methods described here to DSSC that utilize cobalt(II)-bis[2,6-bis(1′-butylbenzimidazol-2′-yl)pyridine[16] as a redox mediator.

Acknowledgment. This work was supported by the University of Bath and Johnson Matthey. The authors thank Jason Riley (University of Bristol) for access to the ellipsometer, Dr. Mike Bailes for technical support, and Jessica Krüger for useful discussions and practical assistance.

References and Notes

(1) O'Regan, B.; Grätzel, M. *Nature* **1991**, *353*, 737.
(2) Grätzel, M. *Prog. Photovoltaics* **2000**, *8*, 171.
(3) Grätzel, M. *J. Sol−Gel Sci. Technol.* **2001**, *22*, 7.
(4) Bach, U.; Lupo, D.; Comte, P.; Moser, J. E.; Weissortel, F.; Salbeck, J.; Spreitzer, H.; Grätzel, M. *Nature* **1998**, *395*, 583.
(5) Kruger, J.; Plass, R.; Cevey, L.; Piccirelli, M.; Grätzel, M.; Bach, U. *Appl. Phys. Lett.* **2001**, *79*, 2085.
(6) Nusbaumer, H.; Moser, J. E.; Zakeeruddin, S. M.; Nazeeruddin, M. K.; Grätzel, M. *J. Phys. Chem. B* **2001**, *105*, 10461.
(7) Tributsch, H. *Appl. Phys. A: Mater. Sci. Process.* **2001**, *73*, 305.
(8) Gregg, B. A.; Pichot, F.; Ferrere, S.; Fields, C. L. *J. Phys. Chem. B* **2001**, *105*, 1422.
(9) Kavan, L.; Grätzel, M. *Electrochim. Acta* **1995**, *40*, 643.
(10) Zaban, A.; Aruna, S. T.; Tirosh, S.; Gregg, B. A.; Mastai, Y. *J. Phys. Chem. B* **2000**, *104*, 4130.
(11) Duffy, N. W.; Peter, L. M.; Rajapakse, R. M. G.; Wijayantha, K. G. U. *Electrochem. Commun.* **2000**, *2*, 658.
(12) Kambili, A.; Walker, A. B.; Qiu, F. L.; Fisher, A. C.; Savin, A. D.; Peter, L. M. *Physica E* **2002**, *14*, 203.
(13) Özsan, M. E.; Johnson, D. R.; Sadeghi, M.; Sivapathasundaram, D.; Goodlet, G.; Furlong, M. J.; Peter, L. M.; Shingleton, A. A. *J. Mater. Sci.-Mater. Electronics* **1996**, *7*, 119.
(14) Fisher, A. C.; Peter, L. M.; Ponomarev, E. A.; Walker, A. B.; Wijayantha, K. G. U. *J. Phys. Chem. B* **2000**, *104*, 949.
(15) Cameron P. J.; Peter, L. M. In preparation.
(16) Nusbaumer, H.; Moser, J. E.; Zakeeruddin, S. M.; Nazeeruddin, M. K.; Grätzel, M. *J. Phys. Chem. B* **2001**, *105*, 10461.